JOURNAL OF PROPULSION AND POWER
Vol. 14, No. 1, January–February 1998

Numerical Investigation of Inlet Buzz Flow

Pong-Jeu Lu* and Ling-Tzong Jain†
National Cheng Kung University, Tainan 70101, Taiwan, Republic of China

The present research aims at developing a time-accurate, high-resolution total variation diminishing scheme and a data-processing procedure that can analyze the inlet buzz flow problem. Special care has been exercised on the numerical buzz flow initiation procedure to minimize the generation of spurious numerical waves. A 10-ft ramjet engine was adopted as the simulation model. The simulated results show that the buzz cycle is attributed both to the local flow instability around the entrance and to the acoustic resonance modes appearing inside the plenum chamber. A revised upstream feedback mechanism is proposed in the present work. It was found that the feedback loop for the subcritical operation is established locally around the inlet region, in which the reflected acoustic waves were sent upstream as a result of the impingement of the shock-induced separation vorticities on the centerbody surface and/or the cowl lip. For the supercritical operation, however, the formation of the feedback mechanism is ascribed to the fundamental acoustic resonance mode generated in the plenum chamber.

I. Introduction

SUPERSONIC inlet is designed to efficiently reduce the flow velocity relative to the engine so that the burning in the combustion chamber may remain stable. However, experiences show that undesired buzz phenomenon may sometimes arise in the subcritical operation condition, leading to combustion instability, engine surge, and/or thrust loss, which result in deterioration of the performance of the propulsion system. A serious buzz phenomenon can even lead to the destruction of the engine. Although buzz has been known since the early design of the ramjet engine,[1] the physical characteristics involved have not yet been thoroughly understood. The explanation of the physical mechanism was based primarily on limited experimental measurements[2–4] assisted by linear analyses.[5,6] Basically, the model and the fluid flow were highly idealized, which failed to give a precise account of the entire physical picture.

Inlet buzz can be categorized as one of the many self-excited flows that occur in fluid dynamics. Excellent reviews on self-excited flows[7–9] are available. In general, the incompressible or the low-speed self-excited flows are comparatively better understood than those of the high-speed flows. It is generally agreed that a self-excited flow must be formed in a closed-loop manner, which consists mainly of two mutually interactive elements, namely, an origin of instability with an associated downstream propagated instability wave, and an upstream feedback mechanism. The acoustic wave often plays the role of upstream feedback because the entropy and vorticity waves are convective waves that flow downstream with the stream. For supersonic inlet flow, these basic elements and their interactions are not clearly defined: the origin of the instability wave (the shock-induced separation point) is moving, the sources of the upstream propagated acoustic wave are hard to define, and how the acoustic resonance of the internal flow affects the system dynamics is not fully understood, leading to a situation that is very difficult to analyze in a straightforward way.

Buzz is generally categorized into two types; the Dailey type[3] and the Ferri type.[2] The Dailey type,[3] which is the main concern of the present study, is typified by the centerbody flow separation and its interaction with the duct acoustic resonance. The present work attempts to analyze this Dailey inlet buzz flow[3] numerically. Advantage will be taken of the abundant data obtained in the simulation. The underlying physics will be disclosed using various data-processing techniques supplemented by the available experimental results.

The Navier–Stokes computations concerning the unsteady inlet buzz flow were first conducted by Newsome[10] using the MacCormack explicit scheme. Buzz flow was obtained only for the closed-end case in which the traveling shock and the high-frequency oscillation were seen. Unfortunately, the computed high-frequency oscillation was found to be associated with the first duct acoustic mode (f = 127 Hz), contrary to the experimental result of the third mode (f = 391 Hz). The reason for this frequency mismatch of the numerical and experimental results was not explained. Moreover, there exists no detailed data analysis to justify how waves may interact and why buzz flow was not observed for the near-critical numerical simulation case, while a 110-Hz high-frequency flow oscillation was observed in the experiment.

Shigematsu and Yamamoto[11] also performed an inlet flow calculation by using a flow plug in the rear of a two-dimensional ramjet to facilitate the control of the back pressure and the mass flux. Numerical results showed reasonably good prediction of the steady-state centerbody surface pressure distributions as compared to the experimental data. As the flow plug is largely closed, unsteady buzz flow was observed in the experiment, whereas there were no results reported about the corresponding numerical simulation. Although unsteady inlet flow phenomena were found occurring in some of the numerical simulations, there existed no accompanying experimental data to compare with. The correctness of the numerical simulation, in particular those of the unsteady flows, hence cannot be evaluated properly.

These numerical simulations indicate that analyzing buzz flow by means of numerical approach is promising but immature. There still exists room for improvements on, at least, the accuracy of the scheme and the numerical procedure of buzz flow initiation. Dailey's experiment,[3] to the knowledge of the authors, is the most thorough work on inlet buzz that can be found in the open literature. It is for this reason that Dailey's work[3] was reinvestigated numerically. Critical numerical procedures leading to buzz flow were carefully examined first. The buzz flow simulations were then performed with the computed results compared to the experimental data.

Received Dec. 6, 1996; revision received Aug. 29, 1997; accepted for publication Sept. 2, 1997.

*Professor, Institute of Aeronautics and Astronautics. E-mail: pjlu@mail.ncku.edu.tw. Senior Member AIAA.

†Graduate Student, Institute of Aeronautics and Astronautics.

Finally, a revised buzz flow mechanism is proposed, which is an outcome based on the numerical results observed.

II. Numerical Methods

A. Governing Equations

In the inlet flow simulations, experiences show that viscous effects are very important. This is because the boundary-layer effects and the flow separation phenomenon are very influential on the internal flow developments. For the present study, the Reynolds-averaged Navier–Stokes equations are adopted as the governing equations which, for the axisymmetric flow, can be written in a compact integral form

$$\frac{\partial}{\partial t}\int_V Q\,\mathrm{d}V + \oint_S n\cdot\boldsymbol{F}\,\mathrm{d}S = \oint_S n\cdot\boldsymbol{F}_v\,\mathrm{d}S + \int_V H\,\mathrm{d}V \tag{1}$$

in which the variables V and S are the control volume and the control surface, respectively, and the conservation variable Q is defined by

$$Q = \begin{bmatrix} e \\ \rho \\ \rho u \\ \rho v \end{bmatrix} \tag{2}$$

where e is the internal energy, ρ is the density, and u and v are the velocity components in the Cartesian x and y directions in the symmetry plane. The convective and viscous flux terms $\boldsymbol{F}$ and $\boldsymbol{F}_v$ are defined, respectively, by the column vectors

$$\boldsymbol{F} = E\boldsymbol{i} + F\boldsymbol{j}, \qquad \boldsymbol{F}_v = E_v\boldsymbol{i} + F_v\boldsymbol{j} \tag{3}$$

The convective fluxes, E and F, are the components of the flux vector $\boldsymbol{F}$ in the x and y directions, which can be expressed as

$$E = \begin{bmatrix} e(u-u_g)+pu \\ \rho(u-u_g) \\ \rho u(u-u_g)+p \\ \rho(u-u_g)v \end{bmatrix}, \qquad F = \begin{bmatrix} e(v-v_g)+pv \\ \rho(v-v_g) \\ \rho v(v-v_g) \\ \rho v(v-v_g)+p \end{bmatrix} \tag{4}$$

In the preceding notations, p is the static pressure, and u_g and v_g are the velocity components of the control surfaces. These control surface velocity terms are required when a dynamic mesh system is used for the initiation of the buzz flow. The mesh movement, hence the cell velocity V_g $(=u_g\boldsymbol{i} + v_g\boldsymbol{j})$, should satisfy the geometric conservation law[12]:

$$\frac{\partial}{\partial t}\int_V \mathrm{d}V + \oint n\cdot V_g\,\mathrm{d}S = 0 \tag{5}$$

The definitions of the viscous fluxes $\boldsymbol{F}_v$ and the source term H appearing on the right-hand side of Eq. (1) were detailed in Ref. 13. To close up the preceding Navier–Stokes equations, the following thermodynamic equation of state is used:

$$p = (\gamma - 1)[e - \tfrac{1}{2}\rho(u^2 + v^2)] \tag{6}$$

The viscosity is assumed to be temperature-dependent only, defined using Sutherland's equation.

By an appropriate nondimensionalization, i.e., using a representative length scale l of the flowfield, the freestream sound speed c_∞ as the reference velocity, and a time scale l/c_∞, and noting that the density ρ and viscosity μ can be nondimensionalized by their freestream values, and the pressure p and internal energy e by $\rho_\infty c_\infty^2$, respectively, Eq. (1) can be rewritten in the original form, except that the viscous fluxes E_v and F_v are modified to take the following forms:

$$E_v = \frac{1}{Re}\begin{pmatrix} \dfrac{\mu}{Pr}T_x + u\sigma_{xx} + v\sigma_{xy} \\ 0 \\ \sigma_{yx} \\ \sigma_{yy} \end{pmatrix}$$

$$F_v = \frac{1}{Re}\begin{pmatrix} \dfrac{\mu}{Pr}T_y + u\sigma_{yx} + v\sigma_{yy} \\ 0 \\ \sigma_{yx} \\ \sigma_{yy} \end{pmatrix} \tag{7}$$

in which the Reynolds and Prandtl numbers and the normalized viscosity are defined, respectively, by

$$Re = \rho_\infty l c_\infty/\mu_\infty, \qquad Pr = C_p\mu/k, \qquad \mu = \mu/\mu_\infty \tag{8}$$

The definitions of temperature gradients T_x and T_y and the stresses $\sigma_{ij}(i, j = x, y)$ can be found in Ref. 13.

Because for massively separated flows there is no conclusive superiority that can be claimed for using a certain turbulence model, we simply used the Baldwin–Lomax algebraic model[14] to approximate the turbulence behavior. In our buzz flow tests, we also tried laminar simulation by switching off the turbulence model and the results, for a global view, showed no significant differences. The problem of turbulence modeling in shock-induced separated flow is important and should not be overlooked. Nevertheless, it goes beyond the scope of the present research.

B. Finite Volume Scheme

In the finite volume approach, the volume integral, Eq. (1), as applied to a finite control volume $V_{i,j}$, can be written as

$$\frac{\partial}{\partial t}\int_{V_{i,j}} Q\,\mathrm{d}V + \oint_{S_{i,j}} n\cdot\boldsymbol{F}\,\mathrm{d}S = \oint_{S_{i,j}} n\cdot\boldsymbol{F}_v\,\mathrm{d}S + \int_{V_{i,j}} H\,\mathrm{d}V \tag{9}$$

Using appropriate spatial discretization, Eq. (9) can be replaced by a semidiscretized equation

$$\frac{\partial}{\partial t}Q_{i,j}V_{i,j} + \sum_{k=1}^{4}(\hat{F}^k_{i,j} - \hat{F}^k_{v_{i,j}}) = H_{i,j}V_{i,j} \tag{10}$$

where k represents the four surfaces of each cell. Cell-averaged $Q_{i,j}$ is assumed to be located at the cell centroid, and $\hat{F}^k_{i,j}$, $\hat{F}^k_{v_{i,j}}$ are the normal numerical fluxes approximated at the kth cell boundary.

The spatial accuracy of the finite volume discretization depends on the construction of the numerical fluxes $\hat{F}^k$ and $\hat{F}^k_v$. In the present study, a modified Osher–Chakravarthy MUSCL-type upwind total variation diminishing (TVD) scheme[15] constructed using the Roe splitting[16] is adopted (see Ref. 17 for nomenclature):

$$Q^-_{m+1/2} = Q_m + \sum_i c_m\left[(a_m + 2\phi b_m)\bar{\alpha}^i_{m+1/2} + \left(\frac{1-2\phi b_m}{a_m}\right)\bar{\bar{\alpha}}^i_{m-1/2}\right] r^i_m \tag{11a}$$

$$Q^{+}_{m-1/2} = Q_m - \sum_i c_m \left[(a_m - 2\phi b_m)\bar{\alpha}^i_{m+1/2} + \left(\frac{1 + 2\phi b_m}{a_m} \right) \bar{\bar{\alpha}}^i_{m-1/2} \right] r^i_m \tag{11b}$$

This scheme was developed particularly for coping with the acoustic wave simulations.[17] The enforcement of this high-resolution scheme on the dynamic grid was also achieved.[18] This newly developed TVD scheme takes into account the grid nonuniformity effect so that the generation of spurious numerical waves can be minimized during computation.[17]

The system of ordinary differential equations, Eq. (10), can be integrated using an explicit three-stage Runge–Kutta scheme,[19] which has been justified to be of second-order accuracy in time while maintaining the TVD property.

C. Boundary Condition Treatments

For numerical inviscid/viscous wall boundary condition implementation, usually the wall pressure is derived from the governing equations subject to the specified wall (physical) boundary conditions. Conventionally, the grids are very clustered in the boundary-layer region for viscous simulations; therefore, the use of $\partial p/\partial n = 0$ to extrapolate the wall pressure from adjacent cell-centered values is satisfactory. Here, in our buzz flow calculations, the boundary-layer approximation often does not hold because massive flow separation may occur as a result of strong shock-boundary-layer interaction effect. Owing to this fact, the wall pressure distribution, in the present viscous and inviscid calculations, was extrapolated using the pressure gradient derived from the momentum equations.

Considering the most general case of a moving wall with surface blowing or suction applied (this can be thought of as a ramjet undergoing maneuvering while the inlet surface bleed flow control is in action), the transverse pressure gradient $\partial p/\partial \eta$ can be expressed as

$$\rho \left(\frac{\partial V_n}{\partial \tau} - \eta_{\tau\tau} - u \frac{\partial \eta_x}{\partial \tau} - v \frac{\partial \eta_y}{\partial \tau} \right) + \rho V_t(\eta_x u_\xi + \eta_y v_\xi) + \rho V_n(\eta_x u_\eta + \eta_y v_\eta) = -\left[(\xi_x \eta_x + \xi_y \eta_y) \frac{\partial p}{\partial \xi} + (\eta_x^2 + \eta_y^2) \frac{\partial p}{\partial \eta} \right] + (\eta_x I_u + \eta_y I_v) \tag{12}$$

where (ξ and η) are grid coordinates and I_u and I_v are the viscous terms

$$I_u = \frac{1}{Re} \left(\frac{\partial \sigma_{xx}}{\partial x} + \frac{\partial \sigma_{xy}}{\partial y} \right) \tag{13a}$$

$$I_v = \frac{1}{Re} \left(\frac{\partial \sigma_{xy}}{\partial x} + \frac{\partial \sigma_{yy}}{\partial y} \right) \tag{13b}$$

In Eq. (12), terms associated with the time derivative $\partial/\partial\tau$ come from the unsteady and/or the dynamic grid effect.[18] The normal and tangential controvariant velocities V_n and V_t are given, respectively, by

$$V_n = \eta_\tau + \eta_x u + \eta_y v, \qquad V_t = \xi_\tau + \xi_x u + \xi_y v \tag{14}$$

The case of $V_n \neq 0$ represents the fact that surface blowing or suction is applied, and that the tangential velocity V_t must be extrapolated from inside the computational domain. As wall Cartesian velocity components are determined using Eq. (14), all of the gradient terms of u and v in Eq. (12) can be approximated. Density ρ is usually extrapolated from the interior neighboring cell-centered values. With all the terms in Eq. (12) being properly approximated using appropriate difference formulas, the transverse pressure gradient $\partial p/\partial \eta$ is, hence, available and the surface pressure can readily be extrapolated.

The inflow and outflow conditions are treated using standard nonreflective characteristic-based boundary condition treatment.[20,21] In the present simulations, this consideration of nonreflective boundaries becomes a bit trivial because the inflow is given supersonic and the outflow, except during the transient startup stage, is supersonically discharged because the downstream throat is seen choked when buzz occurs.

III. Dailey-Type Inlet Buzz Flow

A. Physical Description

One of the ramjet engines that Dailey used for his buzz flow study[3] is shown in Fig. 1. In Dailey's experiments,[3] the shock on the centerbody of the supersonic ramjet engine oscillated when buzz was initiated. The subcritical operation was interrupted when the inlet shock moved upstream to the tip of the centerbody. High-frequency oscillations (the characteristics of low-mass flow period) were observed during the subcritical operation. By the end of these high-frequency oscillations, the inlet shock moved back into the cowl with air ingested at the supercritical rate. According to Dailey's explanation,[3] the subcritical operation was initiated by the blockage of the inlet because of the shock-induced flow separation occurring on the centerbody ramp, which causes the centerbody shock to be expelled upstream to the cone tip and thus deflects the approaching flow away from the cowl lip. During this inlet blockage stage, the downstream air column in the plenum chamber continued to discharge out of the exit nozzle. As the stored mass reduced as a result of the discharge of the air out from both ends of the engine, the plenum chamber pressure became low and the expelled shock waves moved back into the inlet duct and the supercritical operation took over. During the supercritical operation, the mass flux flowing into the inlet was greater than the exit discharge rate, and the plenum chamber was therefore filled up with pressure buildup until the shock was expelled upstream to the inlet ramp, returning to the original subcritical operation condition. This explanation was given by Dailey to describe the buzz cycle he observed.

Dailey's explanation about the inlet buzz was made based on four pressure transducer measurements and high-speed schlieren photography.[3] Although detailed flow structures were not available at that time, the correct overall description of the buzz phenomenon was given. Subsequent studies basically followed Dailey's footsteps,[3] elaborating mainly on the downstream acoustic resonance effect. As a result, the discrete duct resonance frequencies can be predicted using a one-dimensional model, but no assertion can be made on which natural frequency should be associated with the low-frequency buzz cycle. The reason is understandable, because the unsteady shock-induced separated boundary-layer flow around the inlet ramp was too difficult to analyze, making the upstream instability flow part missing from the theoretical modeling of this acoustic resonance phenomenon.

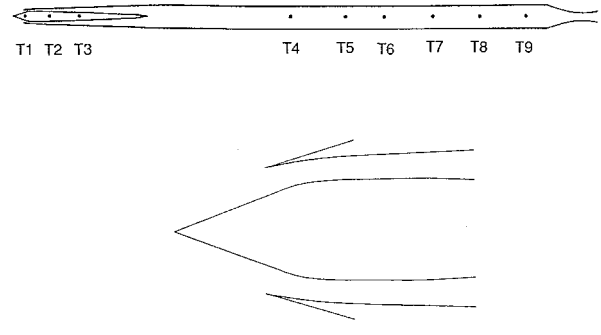

Fig. 1 Ramjet engine configuration and the pressure recording locations (T1–T9).

In the following, a brief introduction of the acoustic resonance modes is given first to explain the role of diffuser plenum chamber on the buzz dynamics. Then numerical simulations of organ-pipe type duct acoustics were performed to shed light on the numerically captured acoustic field. The effects contributed by the inlet flow structures, which would be explained using the concept of entrance acoustic impedance, were demonstrated in these organ-pipe simulations. Finally, one of Dailey's ramjet engines[3] was used to illustrate the numerical simulation and the data analysis method. Discussions of the inlet buzz mechanism were then made based on these computed and processed results.

B. Duct Acoustic Modes

The flow velocity in the diffuser and plenum chamber is low, which allows the use of acoustic equations to be formulated on the basis of a quiescent mean flow. For a one-dimensional, constant cross-sectional pipe, the governing acoustic equation for the pressure perturbation is

$$\frac{1}{c^2}\frac{\partial^2 p'}{\partial t^2} - \frac{\partial^2 p'}{\partial x^2} = 0 \tag{15}$$

where c is the sound speed, and $x = 0$ and $x = L$ correspond, respectively, to the inlet and exit positions of this pipe.

The downstream exit can be taken as a closed end because flow is choked as buzz occurs. The boundary condition specified at the upstream end usually is not known a priori. If the inlet is taken as closed, which models the inlet blockage during the subcritical operation, an infinitely large acoustic impedance is usually specified at $x = 0$, and this will result in an even-mode duct resonance frequency

$$f_n = 2n(c/4L) \quad \text{(even mode)} \tag{16}$$

During the fill-up stage of the Dailey buzz cycle,[3] the entrance impedance is so low that one can use a vanishing impedance condition to approximate it. Using such a boundary condition specification, an odd-mode resonance frequency would take place

$$f_n = (2n - 1)(c/4L) \quad \text{(odd mode)} \tag{17}$$

As the pipe entrance is open to allow the fluid flow in and out, the impedance depends on the local flow structures and usually does not vanish. In what way the resonance condition occurs, in fact, depends on the dynamic characteristics of the surrounding flowfield interfaced with the pipe ends. There are several examples illustrating the resonant, but nonvanishing, local impedance, open-end pipes.[22] In those situations, the pipe length L was modified to account for the nonvanishing resonance impedance and a so-called effective length L_{eff} was used to redefine the resonance frequencies. Similar argument holds for the nearly closed-end case where the impedance is large but still finite.

For the inlet buzz flow problem, a very complicated flow situation occurs in the upstream inlet region. The shock movement and the shock-induced separated vortical flow together make the entrance impedance of the pipe flow hard to predict. Roughly speaking, during the subcritical stage, the plenum pressure is high and the velocity around the inlet is low, yielding a high entrance impedance condition. During the fill-up stage, flow is accelerated into the plenum chamber so that a low impedance may result from the low pressure and high velocity condition at the entrance of the plenum chamber. This explains why both even and odd modes appear in the spectra of the measured buzz pressure.

This complicated upstream flow structure, in principle, can be lumped into a simple entrance-impedance concept as one wishes to analyze the buzz phenomenon via a one-dimensional duct acoustic model. The inclusion of the entrance impedance stresses that the duct acoustic mode analysis should not leave aside the upstream flow dynamics. In the past, the theoretical works all treated the plenum chamber as an independent mechanism that generates even or odd resonance modes. Moreover, the duct modes were taken as the excited responses forced by the turbulent eddies convected from the upstream. It is proposed here that the acoustic analysis should take into account the upstream dynamics. The upstream dynamics may enter in through the boundary condition specification, namely the introduction of the inflow impedance. However, the dilemma is that usually this inlet flow impedance is not obtainable in advance. In other words, a one-dimensional acoustic model described by Eqs. (15–17) can only serve as a conceptual tool, indicating the appearance of acoustic resonance modes. It will be shown in the subsequent organ-pipe buzz flow simulations that, for pipes with equal length but different inlet shape, the computed acoustic resonance modes will show frequency shifts as compared to the frequencies expressed in Eqs. (16) and (17).

IV. Organ-Pipe Flow Simulation

To see whether the high-frequency oscillation can be simulated properly by the present numerical scheme, the same shortened Dailey engine[3] (1.89 ft) as used in the experiment was selected as the model to be computed. Figure 2 illustrates this pipe configuration, which is the Dailey ramjet engine[3] with the centerbody removed and rear exit closed. This closed-end pipe was used by Dailey[3] to represent the chocked mass flux condition for a subcritical operation. During computations, there were seven pressure histories that were recorded at the locations denoted, respectively, by T1, T2, . . . , and T7 as sketched in Fig. 2. Note that the cowl lip is sharp and convex, which makes vortices easily shed as flow oscillates around the cowl lip edge. This vorticity shedding effect was noted by Dailey[3] as the acoustic forcing source in exciting the duct resonance modes.

It is interesting to know how important this vorticity shedding is on the duct resonance phenomenon. A specially de-

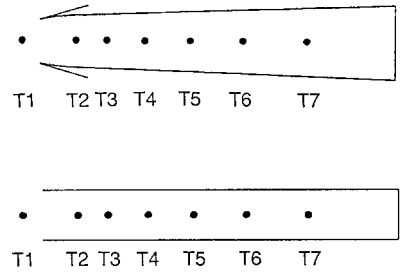

Fig. 2 Dailey's orange pipe and the constant cross-sectional pipe. Pressure histories are recorded at locations T1–T7.

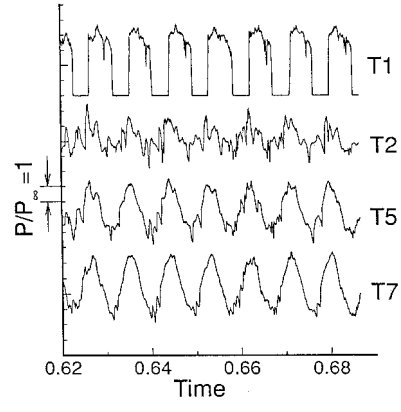

Fig. 3 Pressure histories recorded at T1, T2, T5, and T7 (Dailey's organ pipe).

signed numerical experiment was therefore performed, in which the vorticity generation mechanism was intentionally inhibited. This is done by, first, using an inviscid Euler flow model to reduce the vortical layer development along the pipe wall and, second, adopting a constant cross-sectional pipe configuration to reduce the flow separation around the cowl lip. Acoustic waves can still be well represented in this constant cross-sectional, inviscid model because acoustic resonance is basically an inviscid phenomenon.

Numerical computations were performed to simulate these pipes immersed in a freestream of Mach number 2. The unsteady flows were all started from their original steady-state flows where the downstream ends were open initially. These steady-state pipe flows were all supersonic, and at some instant the exits were suddenly closed and the impulsively generated shocks were seen propagating upstream toward the inlets. For a quite sufficiently long time, the simulations did not reach steady states, but instead, the flows showed persistently oscillatory motions without significant decay. The recorded pressure traces (see Figs. 3 and 4) were Fourier transformed and the spectra are shown in Figs. 5 and 6. It is observed that discrete spikes show up in these spectral diagrams. The two highest energy peaks, 112.2 and 138.7 Hz, were found for the Dailey's[3] and the constant cross-sectional pipes, respectively. These are the fundamental frequencies in which each contains the largest portion of the oscillation energy of the flow.

It was found that the lowest oscillation frequencies, 112.2 and 138.7 Hz, are associated with the oscillatory shock motions. Although both pipes are identical in length, the excited fundamental and higher harmonics are different, indicating the effects contributed by the surrounding inflow dynamics around the inlet. Dailey's organ-pipe[3] generated much more noisy flowfield than did the constant cross-sectional pipe. The much intensified vorticity field around the cowl lip can be reflected from the T2 pressure trace and its spectrum shown, respectively, in Figs. 3 and 5. Relatively irregular pressure fluctuations recorded around the Dailey's pipe and much stronger sideband spectrum around the resonance peaks are the signatures characterizing the turbulence activities associated with the shedding vorticities. The experimental frequency measured by Dailey was 470 Hz, which agrees well with the second peak, 462.8 Hz, of the present Navier–Stokes simulation shown in Fig. 5.

The results of the constant cross-sectional pipe simulation show a closer resemblance to the analytic solutions. Both even and odd resonance modes appear in the spectrum. The disappearance of the high-frequency modes in the downstream is attributed to the less intensified turbulent forcing level and the numerical dissipation contained therein. The low-energy sideband spectra come from the convected vorticities shed from the inlet lip, which should not be mistaken for the numerical

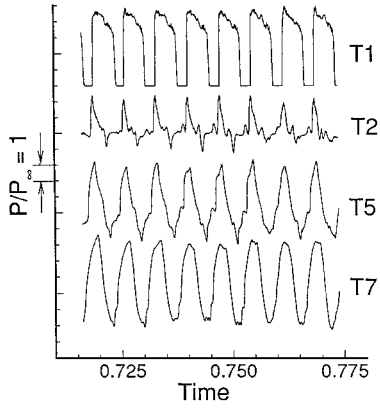

Fig. 4 Pressure histories recorded at T1, T2, T5, and T7 (constant cross-sectional pipe).

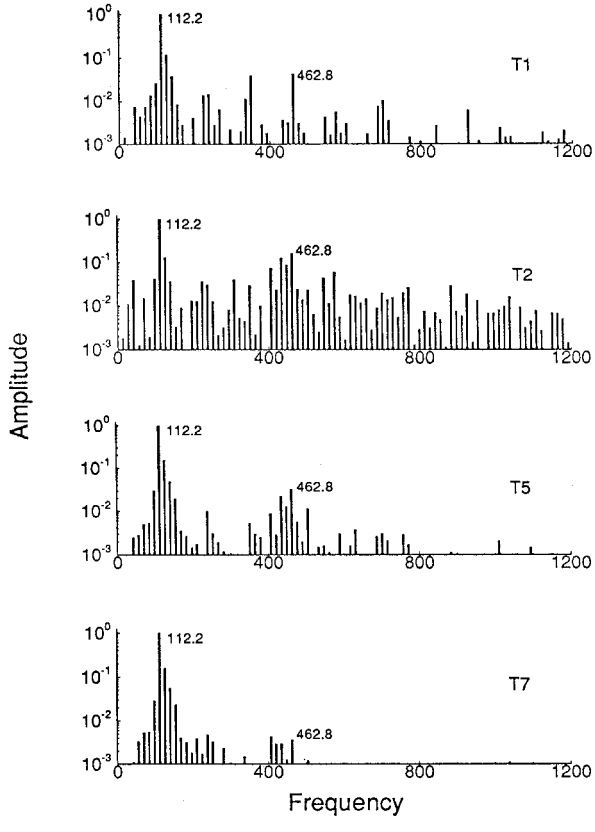

Fig. 5 Spectra of pressure histories recorded at T1, T2, T5, and T7 (Dailey's organ pipe).

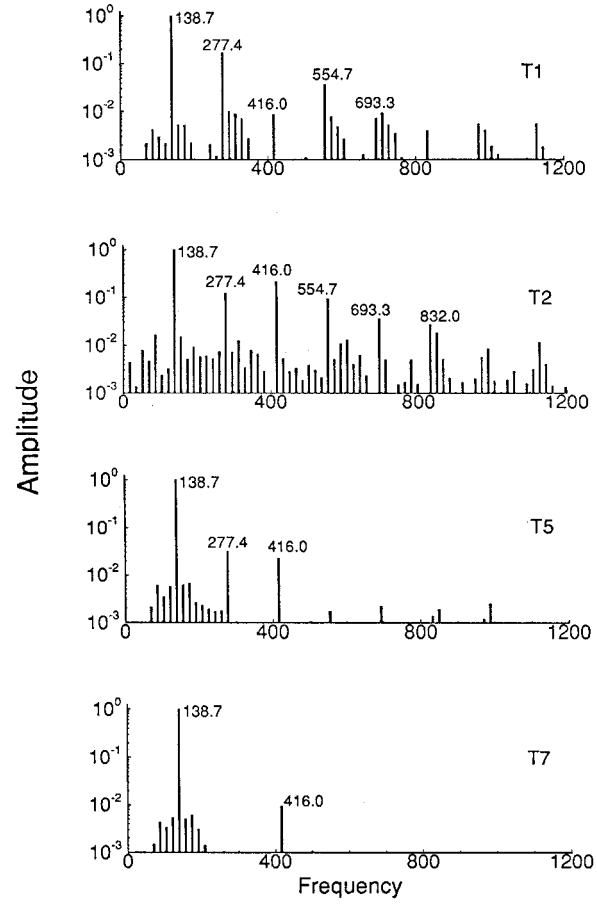

Fig. 6 Spectra of pressure histories recorded at T1, T2, T5, and T7 (constant cross-sectional pipe).

error. (A controlled numerical experiment of this constant area pipe, with both ends closed, was carried out. The results show isolated, pure-tone type spikes distributed on the spectrum.) Comparing Figs. 5 and 6, it is observed that Dailey's spectrum[3] possesses a preferred mode (462.8 Hz) in the chamber, in contrast to the multiple even and odd coexisting modes of the constant area pipe. This implies that much organized vortices are present in Dailey's pipe, and these shed vortices can pick up in an autonomous manner the mostly excited resonance mode.

Some remarks can be drawn from this organ-pipe flow simulation. First, the present numerical code can resolve sufficiently, although not completely, the acoustic resonance phenomenon in a pipe. Note that this numerical procedure solves the inlet and the downstream acoustic field as a whole. In other words, the feedback loop was naturally accounted for in the simulations. As different inlet shapes, hence different inlet dynamics, are involved, it is found that different resonance frequencies appear, although equal length pipes are being used. This finding is particularly valuable for the subsequent inlet buzz analysis. In the past, resonance in the diffuser was taken as a forced response. Self-sustained instability was thought to be established locally as a forcing mechanism in the upstream inlet zone, and the acoustic modes were excited in the diffuser by the downstream propagated separated vortical flow. This concept makes the past analysis only able to predict discrete resonance frequencies. However, it cannot make any comments about which mode might connect with the low-frequency buzz oscillations of the entire system. The present simulations clearly point out and correct this shortcoming. It is shown that the surrounding inlet dynamics do contribute in determining the duct resonance frequencies, as revealed from the different resonance frequencies found in Dailey's and the constant cross-sectional pipes simulations. The communication connecting the complex upstream inlet flow and the downstream duct acoustic oscillations can be thought of as fulfilled by way of the inlet impedance specification.

V. Dailey Buzz Flow Simulation

The 10-ft ramjet engine used in Dailey's experiment[3] was chosen for the present simulation. The centerbody and cowl lip configuration is shown in Fig. 1. To facilitate the numerical computations, the exit shape was changed using a throat to replace the original conical frustum. This was done by making the rear part of the simulated configuration into a convergent–divergent nozzle. The engine length, 10 ft, is now defined as the distance between the tip of the centerbody and the exit nozzle throat. We chose a 41% captured area (the same as in Dailey's experiment) as the exit throttle condition for the following numerical simulations.

A. Numerical Buzz Onset Procedures

Based on our own experiences, the startup of the present internal flow computations requires careful treatments. To conduct self-sustained flow simulations, we do not want the numerical error signals to be mistaken for the physical waves that travel back and forth in the engine, in particular when the errors are hard to expel or damp out as buzz arises. A way to achieve this purpose is to let the startup procedure be compatible with some practical physical situations. To this end, three methods were designed, and in the following the descriptions of the initiation procedures and the results obtained are detailed.

The first buzz-initiation procedure uses the dynamic grid method to distort the engine wall continuously. Steady-state flow with supersonic outflow was first achieved by letting the diffuser throat fully open. Then the exit throat was gradually squeezed until the desired throat area ratio was obtained. Buzz flow was naturally established and the results are shown in Figs. 7 and 8.

The second initiation procedure started with the use of an inviscid Euler solver and the same dynamic grid method addressed earlier. It is interesting to see that a steady-state inviscid flow was generated. The pattern of a normal shock intersecting with an oblique shock in the inlet region agreed qualitatively with the Dailey's experimental observation.[3] Viscous terms were then added together with grid system refined around the wall region. After the introduction of the viscous effect, the unstable buzz motion appeared, showing a self-excited flow with quite consistent buzz frequency and centerbody shock structure as compared to the experimental and the first startup results.

The reason why buzz flow did not arise in the inviscid flow simulation can be anticipated. This is because the instability origin, namely, the shock-induced boundary separation point and the associated flow structure, was not well accounted for in the inviscid model. This points out the important role of the viscous effects in the inlet buzz flow simulations.

The third buzz flow initiation method imitates the actual physical situation of a supersonic flow ramming into the en-

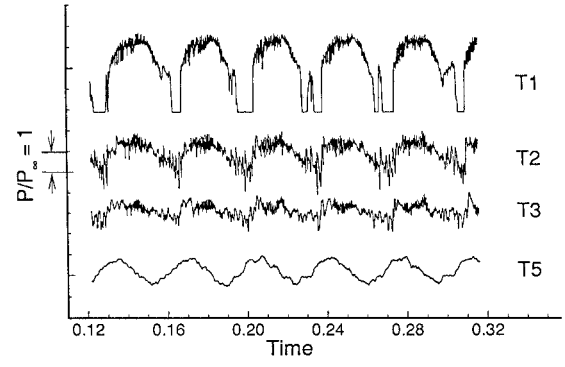

Fig. 7 Pressure histories recorded at four locations of a buzz simulation (the first startup case, engine length 10 ft).

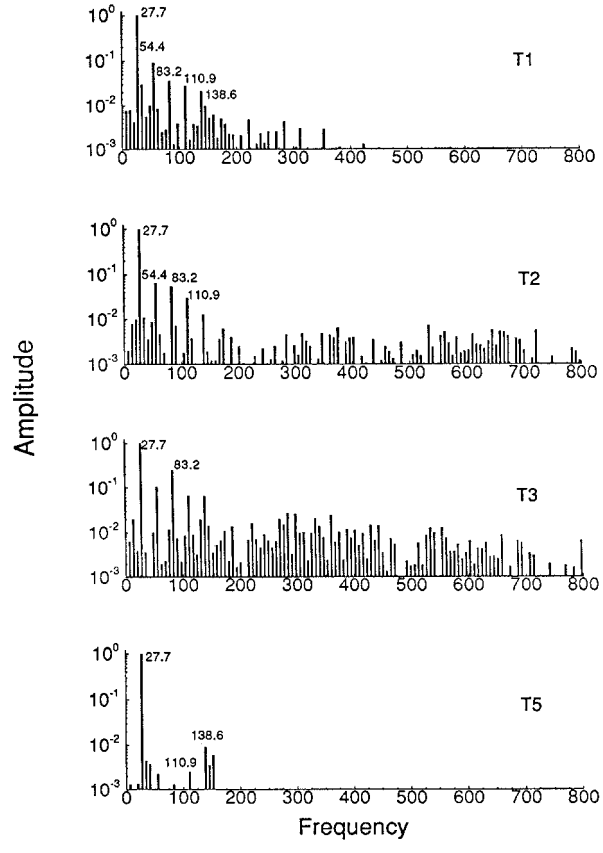

Fig. 8 Spectra of pressure histories recorded at T1, T2, T3, and T5 (the first startup case, engine length 10 ft).

gine. The grid system was kept fixed during the course of computation. The outflow boundary condition was enforced strictly by following the characteristic boundary condition treatment. Before the exit throat was choked, the ambient pressure was used as the specified outflow condition. This subsonic outflow condition treatment was only required for the initial transient flow stage. As buzz flow was established and the exit throat became choked, the supersonic exit flow required no exit boundary condition to be specified.

An examination of the results computed using different start-up procedures shows that, qualitatively, the same type buzz flow was obtained. However, the detailed flow oscillations were neither identical nor repeatable, which indicates that the separated flow was prevailing in these buzz flow structures. The last buzz initiation method took the longest transient time, and the downstream signals, e.g., the T5 trace, were mostly damped owing to the excessively long time of computation. The advantages of using dynamic grid technique for starting the numerical buzz computation, therefore, are demonstrated to be economy and reliability.

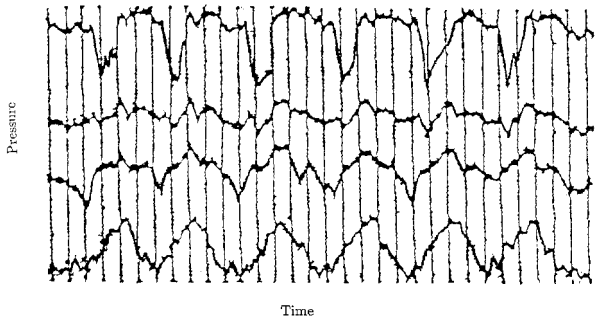

Fig. 9 Experimental pressure measurements during a buzz cycle (adapted from Fig. 9 of Ref. 3).

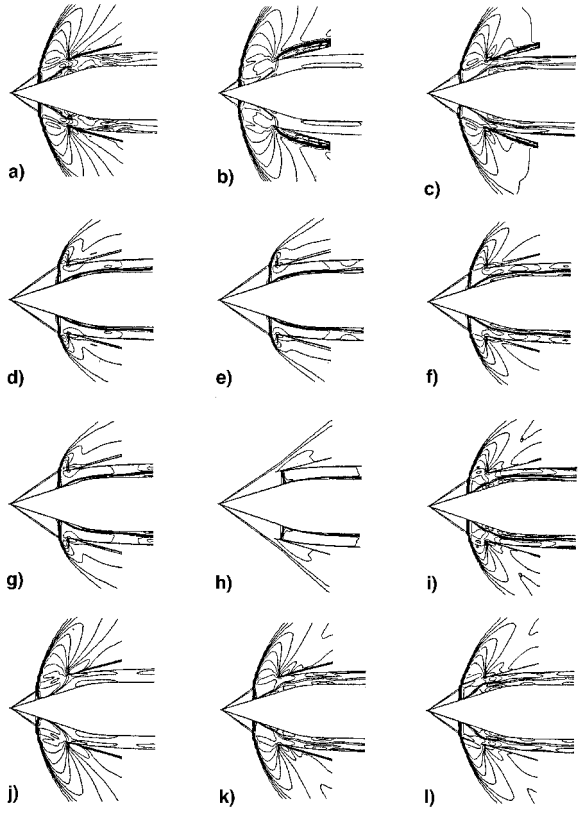

Fig. 10 Mach number contour plots in a buzz cycle.

B. Buzz Flow Structures

First, let us take a look at the pressure histories recorded at T1, T2, T3, and T5 locations. Figure 9 illustrates the experimental pressure traces measured using pressure transducers. Our numerical results are presented in Fig. 7. The overall impression is that the numerical and experimental results behave in a quite similar manner. (Note that the second experimental pressure measurement was not reliable because the pressure transducer was claimed to be broken during the course of the experiment.) The Fourier spectra of these pressure records are shown in Fig. 8. The lowest resonance mode, which encompasses the largest energy content of the oscillating flow, shows a peak frequency around 27.7 Hz. This value agrees quite closely with the experimentally observed 25 Hz. A number of even and odd modes also show up in Fig. 8. This solution characteristic basically complies with the previous organ-pipe results, which indicates the existence of higher resonance modes existing in the diffuser flow. Moreover, the broadband spectra were seen to be comparatively intense in the wake region (T3 probe) where vorticity waves were strong.

Shock motion and inlet flow structures are illustrated in Figs. 10 and 11 using a series of Mach number and vorticity contour plots. These contour plots were taken at 12 instants (Figs. 12a–12l). With the aid of the contour plot presentation, the upstream flow structure and its relationship with the centerbody (T1, T2, and T3) and diffuser (T5) pressure trends can be revealed. It is observed that the general buzz flow picture was captured by the present numerical method when compar-

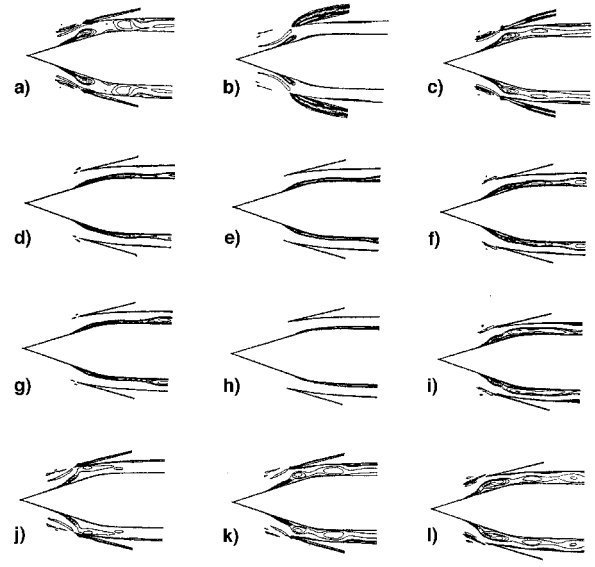

Fig. 11 Vorticity contour plots in a buzz cycle.

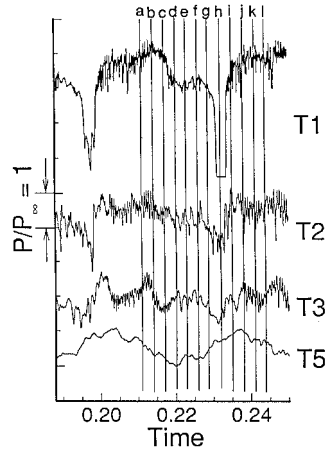

Fig. 12 Instants for snapshots to be taken in a buzz cycle.

ing these snapshots with the experimental high-speed schlieren photographs.

Stages 12a and 12b represent the moment of serious inlet flow blockage caused by the expelling pressure wave sent from the downstream plenum chamber. The flow that is blocked and diverged away from the inlet ramp can be seen from the vorticity plots (Fig. 11) in which the shock-induced flow separation is depicted. As shock continues moving upstream to the tip, the air mass is both spilled away from the inlet and, in the meantime, exhausted through the exit nozzle. The pressure data recorded at T1, T2, and T3 on the centerbody are high (see Fig. 12), however, the pressure at the plenum chamber (T5) shows a declining trend, indicating that the stored air column, at the inlet block stage, is continuously discharged from the exit nozzle. As the T5 pressure reduces to its minimum (stages 12c and 12d), the inlet shock can no longer move upstream and starts to reverse its direction and accelerate toward the downstream cowl lip. Stages 12d–12h represent the fill-up period, and the T5 pressure trace shows an increasing trend, indicating air mass was compressed and stored. Figure 13 shows the instantaneous mass fluxes at 12a–12l. The vertical coordinate is nondimensionalized by the mass flux within the freestream capture area. During the subcritical operation period (stages 12a, 12b, 12j–12l), the inlet has been virtually blocked with extremely low inflow mass flux. This blocked inlet recovers approximately 20% of the capture area mass flux back when the supercritical operation (stages 12d–12h) prevails.

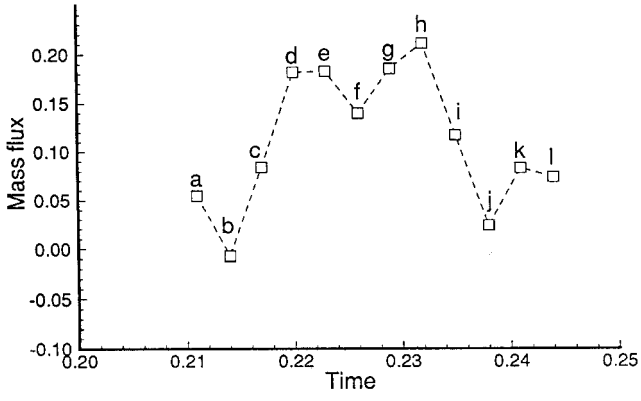

Fig. 13 Instantaneous mass fluxes at the entrance of the inlet in the selected 12 stages.

In the present case, shock is seen completely swallowed into the inlet cowl (see 12h); however, it does not pass through the inlet throat during the supercritical fill-up period. Partly because a shock cannot stably stay on a convergent part of a duct, and partly because of continuingly increasing plenum chamber pressure, the shock starts moving upstream as shown in 12h–12j. A subcritical condition is then resumed together with the high-frequency oscillation setting in.

Figures 14 and 15 portray the spatial–temporal mass flux and the pressure distributions in a buzz cycle. These diagrams provide a system view, which is a convenience enjoyed by the computational fluid dynamics (CFD) simulation, for the inlet buzz analysis. Situations in the plenum chamber are relatively smoother than in the inlet centerbody region. Very irregular flow oscillations are observed in both the mass flux and the pressure diagrams around the inlet, as characterized by the corrugated distribution surfaces. In the diffuser plenum chamber ($4 \leq x \leq 10$), a triple-ridged surface distribution is found for both the mass flux and the pressure distributions. This phenomenon results from the coexistence of the most dominant first two resonance modes ($n = 1, 3$ and $f_1 = 27.7$ Hz, $f_3 = 83.1$ Hz) in the plenum chamber. Note that the second mode ($n = 3$) loses its influence, whereas the fundamental ($n = 1$) mode takes a commanding control over the shock motion around the inlet region. The exit throat is seen choked and the discharged mass flux shows a pretty steady trend in time. It can be concluded that, during the buzz period, the unsteady and turbulent low-frequency mass flux flow dominates primarily in the inlet and the centerbody region, while the higher duct acoustic harmonics are excited by the separated wake convected in the

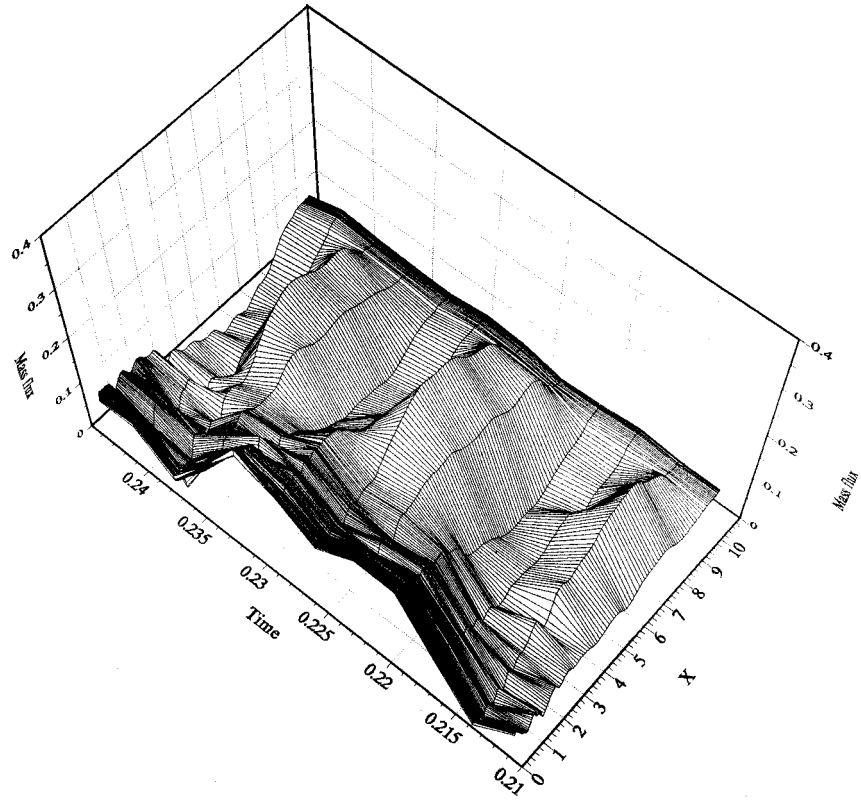

Fig. 14 Spatial-temporal mass flux distributions of the ramjet engine in a buzz cycle.

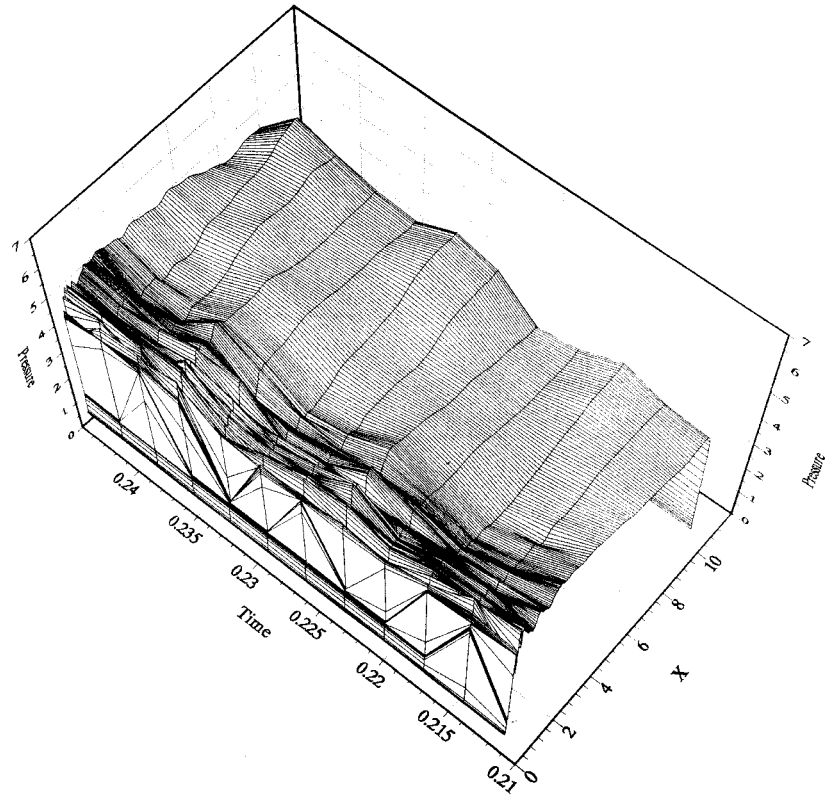

Fig. 15 Spatial-temporal pressure distributions of the ramjet engine in a buzz cycle.

downstream plenum chamber. These upstream and downstream flow interactions communicate in a closed-loop sense, and the inlet oscillatory flow couples with the lowest resonance frequency associated with the downstream plenum chamber.

VI. Buzz Feedback Loop

In principle, self-sustained flow oscillation cannot arise when the resultant event does not link with the cause. The way this upstream cause and downstream event communicate, or the establishment of the so-called feedback loop, holds a central position in the self-sustained oscillating flow studies. In subsonic fluid flows, acoustic waves often play this role of upstream influence. Generally speaking, aside from the mixing flows, the feedback signals that can result in a self-excited flow must be strong and organized. Sound induced by vortical waves impinging on a solid surface is a typical way of generating those feedback signals.[23] Dailey made a judicious argument about the feedback loop for the inlet buzz experiments he performed.[3] He proposed that the buzz instability was caused by the local flow interaction around the entrance of the inlet. The possibility of considering the exit throat as a place to generate feedback signals was ruled out by a simple time scale argument. Dailey also explained that the low-frequency buzz cycle occurred in response to the fill-up action in the plenum chamber.

To extract these sound sources from the simulated results, data processing using the fluctuating dilatation field Δ' can be performed

$$\Delta' = \Delta - \bar{\Delta} \tag{18}$$

$$\Delta = \nabla \cdot \boldsymbol{V} \tag{19}$$

where Δ denotes the divergence of the instantaneous velocity field $\boldsymbol{V}$, and the overbar stands for time average. The intensity of the sound sources in the low-speed fluid flow has been shown to be proportional to the fluctuating dilatation field Δ'.[24,25] Here, in our buzz flow simulations, the period for averaging the time mean value $\bar{\Delta}$ corresponds to the low-frequency (27.7 Hz) mode. Figure 16 shows these fluctuating dilatation Δ' plots of the 12 stages of Figs. 12 and 13. To facilitate the contour plotting work, sound sources in the vicinity of the shock that arise from the shock dipole effect were filtered out. It is observed that strong sound sources can be found at the inlet blockage stages, Figs. 16a–16c, 16h–16l, and the fill-up stages 16h and 16i. The oscillatory forward movement of shock wave during the subcritical inlet blockage period was explained as a result of the local pressure rise around the inlet entrance. Figure 16 justifies this statement by showing that the strong sound sources are produced as the separated vortical structures interact with the cowl and the inlet ramp surfaces. These impinging vorticities may work as a strong dipole sound source[23] and, as feedback to interact with the upstream separation point, will result in a closed-loop, self-excited sawtooth-type high-frequency oscillating flow.

Note that at Fig. 16h, the downstream vorticity field becomes so weakened that the previously mentioned impinging vorticity-induced sound waves almost disappear. The subsequent supercritical fill-up action, and hence the forward shock motion, would not come into existence if there was no other feedback mechanism checked in. It is the plenum chamber fundamental acoustic resonance mode that takes over the role of upstream feedback that resists this fill-up action by generating an expulsive chamber pressure. The massively separated vorticities that revive again, as shown in Fig. 16i, are caused by this pressure expulsion. As separated vorticities enhance and the inlet becomes blocked, the local dipole sound sources are strengthened and the local instability loop forms again, as shown in Figs. 16i–16l.

Hankey and Shang[26] collected a number of inlet buzz flows and found that all the buzz frequencies coincided with the fundamental ($n = 1$) resonance frequencies of the downstream diffuser pipes. This conclusion also agrees with the present organ-pipe and ramjet buzz flow simulations. To further test the validity of this conclusion, we decreased the present ramjet engine length from 10 ft to 8 ft. Similar buzz be-

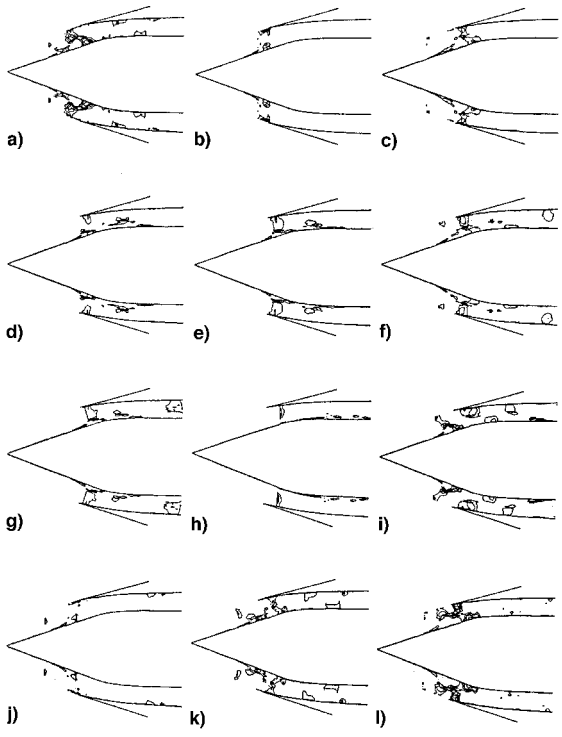

Fig. 16 Fluctuation dilatation fields during a buzz cycle.

havior has been found. However, the buzz frequency is now raised to 32.5 Hz. Because a shorter pipe length leads to a higher resonance frequency, the latter simulation proves that the low-frequency buzz oscillation must be associated with the pipe acoustic resonance waves. Otherwise, the frequency will not be modified if the buzz is merely a local instability phenomenon around the inlet region. This demonstration shows that the acoustic resonance modes must participate in the formation of the feedback mechanism by coupling with the upstream flow dynamics to result in a buzz instability.

In summary, it is presently proposed that there are two feedback loops that alternatively appear in Dailey-type inlet buzz flow.[3] During the subcritical inlet blockage period, the instability of the shock motion is caused by the local separated vortical waves and the induced upstream propagating sound generated around the inlet cowl and centerbody surface. During the supercritical fill-up stage, the shock excursion is associated with the modulation of the chamber pressure contributed by the fundamental acoustic resonance mode of the diffuser plenum chamber.

VII. Concluding Remarks

Dailey-type inlet buzz flow was revisited using time-accurate Navier–Stokes simulations. A high-resolution modified Osher–Chakravarthy upwind TVD scheme and a finite volume method were used. A study on the numerical buzz initiation procedures was made. It was found that viscous effect plays an essential role in generating the buzz instabilities. Care has also been exercised so that the confusion with the spurious numerical waves can be avoided in the present numerical buzz flow investigation. Successful numerical simulations were achieved with results that agreed well with the data obtained from the experiments.

A one-dimensional acoustic wave analysis was established, which served as a theoretical background that guided the following numerical buzz flow simulations. This analysis stresses the idea that in a buzz flow the acoustic resonance is not necessarily an excited response only. Interface impedance, which represents the dynamic effects offered by the surrounding inlet flow, may change the resultant acoustic resonance modes. This closed-loop type view provides valuable guidelines for performing the subsequent numerical buzz simulations and for giving the physical explanations.

Prior to the inlet buzz computations, the organ-pipe oscillatory flow simulations were conducted. The role of vortex shedding from the inlet entrance, and hence the effects provided by the upstream dynamics, were demonstrated. Both spike-like resonance frequencies and broadband vorticity fluctuations were observed. The results agreed favorably with those of Dailey's experiment; hence providing encouraging support for the proposed one-dimensional numerical duct acoustic analysis.

The Dailey's ramjet engine was used for exploring the underlying inlet buzz mechanism. The computed low-frequency buzz of 27.7 Hz agrees well with the experimentally observed 25 Hz. Contour snapshots, spectral analyses, and techniques for extracting the acoustic field have been exploited. All of these data-processing techniques reconfirm experimental findings and provide a more detailed description of the underlying physics.

Dailey was not completely able to explain the role of diffuser resonance in connection with the inlet buzz dynamics. His suggestion that inlet flow breakdown is a local phenomenon pertaining to the entrance flow blockage was modified. By the use of fluctuating dilatation field, at different stages, the feedback loops were demonstrated to be generated from the cowl lip/centerbody surfaces and from the diffuser plenum chamber as well. These two feedback loops were explained here as ascribed, respectively, to the different stages pertaining to the subcritical inlet blockage and the supercritical plenum fill-up operations.

Acknowledgments

This research was partially supported by the National Science Council under Contract NSC 85-2623-D006-023. The authors would like to thank the unknown reviewers for many valuable comments and suggestions.

References

[1]Oswaititsch, K., "Pressure Recovery in Missiles with Reaction Propulsion at High Supersonic Speeds (The Efficiency of Shock Diffuser)," NACA TM-1140 (translation), June 1947.

[2]Ferri, A., and Nucci, R. M., "The Origin of Aerodynamic Instability of Supersonic Inlets at Subcritical Conditions," NACA RM-L50K30, Jan. 1951.

[3]Dailey, C. L., "Supersonic Diffuser Instability," *Journal of the Aeronautical Sciences*, Vol. 22, No. 11, 1955, pp. 733–749.

[4]Nagashima, T., Obokato, T., and Asanuma, T., "Experiment of Supersonic Air Intake Buzz," Inst. of Space and Aeronautical Science, Univ. of Tokyo, Rept. 481, Tokyo, Japan, May 1972.

[5]Mirels, H., "Acoustic Analysis of Ram-Jet Buzz," NACA TM-3574, 1955.

[6]Trimpi, R. L. "A Theory for Stability and Buzz Pulsation Amplitude in Ram Jets and an Experimental Investigation Inducing Scale Effects," NACA Rept. 1265, 1953.

[7]Rockwell, D., and Naudasher, E., "Self-Sustained Oscillations of Impinging Free Shear Layers," *Annual Review of Fluid Mechanics*, Vol. 11, 1979, pp. 67–94.

[8]Rockwell, D., "Oscillation of Impinging Shear Layers," *AIAA Journal*, Vol. 21, No. 5, 1983, pp. 645–664.

[9]Meier, G. E., Szumowski, A. P., and Selerowicz, W. C., "Self-Excited Oscillations in Internal Transonic Flows," *Progress of Aerospace Sciences*, Vol. 27, 1990, pp. 145–200.

[10]Newsome, R. W., "Numerical Simulation of Near-Critical and Unsteady, Subcritical Inlet Flow," *AIAA Journal*, Vol. 22, No. 10, 1984, pp. 1375–1379.

[11]Shigematsu, J., and Yamamoto, K., "A Numerical Investigation of Supersonic Inlet Using Implicit TVD Scheme," AIAA Paper 90-2135, July 1990.

[12]Vinokur, M., "An Analysis of Finite-Difference and Finite-Volume Formulations of Conservation Laws," *Journal of Computational Physics*, Vol. 81, 1989, pp. 1–52.

[13]Jain, L.-T., "On the Numerical Investigation of Inlet Buzz Flow," Ph.D. Dissertation, Inst. of Aeronautics and Astronautics, National Cheng Kung Univ., Tainan, Taiwan, ROC, June 1994.

[14]Baldwin, B., and Lomax, H., "Thin Layer Approximation and Algebraic Model of Separated Turbulent Flows," AIAA Paper 78-257, Jan. 1978.

[15]Chakravarthy, S. R., and Osher, S., "A New Class of High Accuracy TVD Schemes for Hyperbolic Conservation Laws," AIAA Paper 85-0363, Jan. 1985.

[16]Roe, P. L., "Approximate Reimann Solvers, Parameter Vectors and Difference Scheme," *Journal of Computational Physics*, Vol. 43, 1981, pp. 357–372.

[17]Lu, P. J., Pan, D., and Yeh, D. Y., "On the Numerical Simulation of Trailing Edge Acoustic/Vortical Interaction," *AIAA Journal*, Vol. 33, No. 5, 1995, pp. 785–793.

[18]Lu, P. J., Pan, D., and Yeh, D. Y., "Transonic Flutter Suppression Using Active Acoustic Excitations," *AIAA Journal*, Vol. 33, No. 5, 1995, pp. 694–702.

[19]Venkatakrishnan, V., and Jameson, A., "Computation of Unsteady Transonic Flows by the Solution of Euler Equations," *AIAA Journal*, Vol. 26, No. 8, 1988, pp. 974–981.

[20]Thompson, K. W., "Time Dependent Boundary Conditions for Hyperbolic Systems," *Journal of Computational Physics*, Vol. 68, 1987, pp. 1–24.

[21]Hedstrom, G. W., "Nonreflecting Boundary Conditions for Nonlinear Hyperbolic Systems," *Journal of Computational Physics*, Vol. 30, 1979, pp. 222–237.

[22]Kinsler, L. E., Frey, A. R., Coppens, A. B., and Sanders, J. V., *Fundamentals of Acoustics*, 3rd ed., Wiley, New York, 1982, Chap. 8.

[23]Ho, C. M., and Nosseir, N. S., "Dynamics of an Impinging Jet. Part II. The Feedback Phenomenon," *Journal of Fluid Mechanics*, Vol. 105, 1981, pp. 119–142.

[24]Crighton, D. G., "The Excess Noise Field of Subsonic Jets," *Journal of Fluid Mechanics*, Vol. 56, 1972, pp. 683–694.

[25]Jou, W. H., and Menon, S., "Modes of Oscillation in a Nonreacting Ramjet Combustor Flow," *Journal of Propulsion and Power*, Vol. 6, No. 5, 1990, pp. 535–543.

[26]Hankey, W. L., and Shang, J. S., "Analysis of Self-Excited Oscillations in Fluid Flows," AIAA Paper 80-1346, July 1980.